Molecular Crystals and Liquid Crystals
Publication details, including instructions for authors and subscription information:
http://www.tandfonline.com/loi/gmcl16

Vibronic Interactions in the Naphthalene Molecule

John Wessel [a] & Donald S. McClure [b]

[a] Department of Chemistry, University of Chicago, Chicago, Illinois, 60637, U.S.A.

[b] Department of Chemistry, Princeton University, Princeton, New Jersey, 08544, U.S.A.

Version of record first published: 20 Apr 2011.

To cite this article: John Wessel & Donald S. McClure (1980): Vibronic Interactions in the Naphthalene Molecule, Molecular Crystals and Liquid Crystals, 58:1-2, 121-153

To link to this article: http://dx.doi.org/10.1080/01406568008070155

Mol. Cryst. Liq. Cryst., 1980, Vol. 58, pp. 121–153
0026-8941/80/5801-0121$04.50/0

Vibronic Interactions in the Naphthalene Molecule†

JOHN WESSEL‡

Department of Chemistry, University of Chicago, Chicago, Illinois 60637, U.S.A.

and

DONALD S. McCLURE

Department of Chemistry, Princeton University, Princeton, New Jersey 08544, U.S.A.

The second singlet–singlet absorption system of naphthalene ($^1B_{2u}$) has been examined in diverse host media at low temperature. Naphthalene substituted in durene and *p*-xylene crystals reveals hundreds of narrow lines ($w_{1/2} \sim 2\,cm^{-1}$) within the first $1500\,cm^{-1}$ of $^1B_{2u}$. Although the same gross band contours occur in all mixed crystal systems studied, each provided unique internal structure; also each deuterium isotope of naphthalene has a unique internal line pattern.

This complexity is shown to derive from resonant vibronic interference between the $^1B_{2u}$ electronic configuration and the underlying $^1B_{3u}$ vibronic manifold. It is a clear demonstration of the detailed interactions responsible for radiationless processes in such systems. The structure admits to a direct quantitative analysis by means of extended Herzberg–Teller theory and provides coupling terms within such a framework.

INTRODUCTORY NOTE

The subject matter of the following paper is already well known to many people. It is on the interaction between the first and second singlet states of naphthalene from the doctoral thesis of John Wessel.[1] The thesis was read and used widely, and formed the basis of papers by Langhoff and Robinson[2] and by Hong[3] who provided additional analysis of the data. The paper prepared by us had not been published for various bad reasons, but we believe it is still of importance to do so, particularly because of the large amount of

† Supported by a grant from the National Science Foundation. Presented at the 5th Molecular Crystal Symposium, Philadelphia, 1970.

‡ Now at Aerospace Corporation, P.O. Box 92957, Los Angeles, California, 90009.

experimental data it contains which is not generally available, and because there are several interesting aspects of Wessel's analysis which the other analyses have not brought out. The occasion of a memorial to Vladimir Broude provided us with the necessary incentive to finish this work.

D. S. McClure

I. INTRODUCTION

It is now well known that transitions to the second excited singlet state of a large molecule produce a complex spectrum, due in part to the interactions between the first and second excited singlet states. An early example of this complexity was found in the spectrum of naphthalene[4] and is illustrated in Figure 1, the polarized spectrum of naphthalene in an oriented single crystal of durene at 2°K. The B_{2u} spectrum appears only in the short axis polarization cleanly separated from overtones of the long axis B_{3u} spectrum. It is clearly a much more congested spectrum than either the long or short-axis B_{3u} spectrum. The purpose of this paper is to investigate the interaction between the $^1B_{2u}$ and $^1B_{3u}$ states of naphthalene.[1]

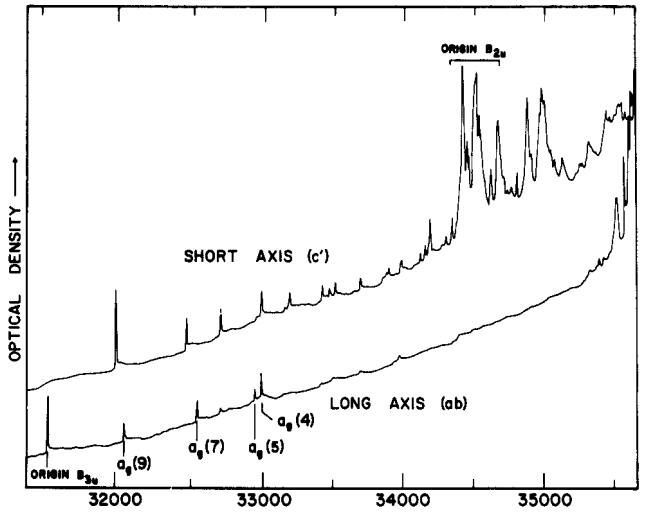

FIGURE 1 The long (*ab*) and short (*c'*) axis polarized absorption spectra of h_8-naphthalene in durene at 2.2°K. The vertical scale is linear in log intensity. No correction has been made for instrumental sensitivity which decreases smoothly with increasing energy, nor for the host transmission, which is uniform below 35,000 cm^{-1}. Long axis lines above 35,500 cm^{-1} are from the durene host. A large effective slitwidth in this figure obscures structure, in the sharp (FWHH $\sim$ 2 cm^{-1}) weak long axis lines within the $^1B_{2u}$ origin region. Also numerous multiplets are obscured. They are more apparent in Figure 3.

This subject is of considerable significance now because of the great current interest in the dynamics of the disposition of electronic energy in molecules. Kasha noted that the fluorescent or phosphorescent emission from molecules in condensed phases occurs from the lowest excited states of the given multiplicity regardless of the energy of excitation.[5] Observations that quantum yields of fluorescence in several cases were nearly the same in the condensed phase as in the vapor led to the suggestion that the processes responsible for energy degradation were intramolecular, and that the nature of the surrounding phase was only of secondary importance.[6] The observation of Williams and Goldsmith on naphthacene showed most clearly that this is the case.[7] They showed that the fluorescence spectra of low pressure vapor in which molecules cannot make collisions before radiating were virtually independent of the wavelength of excitation. Even when excited to the second singlet level, the fluorescence resembled that emitted by the first singlet level. The excess energy remains as vibrational energy after the act of emission. All of the above observations show that higher electronic states interact vibronically with lower ones. The direct spectroscopic observation of this interaction is the subject of this paper.

II. EXPERIMENTAL

The naphthalene-h_8 was zone refined a minimum of 100 passes. Since the $^1B_{2u}$ system is intense and allowed, additional purification for these mixed crystal absorption studies was unnecessary. The *d*-8, naphthalene was obtained from Merck and Company Ltd., Canada, the 1,4,5,8-d_4 and 2,3,6,7-d_4 was kindly supplied by Professor C. A. Hutchinson. These were purified by gas–liquid chromatography on a 5000 plate silicone oil column. Durene transparent to 2800 Å was obtained by purification of Eastman and of Baker reagent materials. Most batches of material required treatment with 2,4-diphenylhydrazine hydrochloride and subsequent zone refining. The *p*-xylene was purified by liquid chromatography on a $\frac{1}{2}$ in column packed with one foot alumina followed by one foot silica gel. Toluene and *n*-pentane hosts were Matheson, Coleman and Bell spectra quality reagents.

Crystals of durene and *p*-xylene were grown by the Bridgman technique. Durene was grown in vacuo, *p*-xylene under atmospheric conditions. Spectral line width in the $^1B_{3u}$ origin varied from 0.5 to 2.0 cm^{-1} among crystals grown from identical melts. Since the molecular linewidths in the $^1B_{2u}$ system were always 2 cm^{-1} or broader, such effects were not important to these studies. (No variation was observed for line widths in the resonance region) Measurements were made at 2.2°K on crystals immersed in liquid helium. A 2200 watt compact arc DC xenon source, filtered by a $NiSO_4$ solution and

Corning 7-54 filter provides the background source. A 3.4 meter Jarrell-Ash spectrograph fitted with a 1200 line/mm replica grating was used in first order. Photoelectric measurements with resolution 60,000 were recorded as the logarithm of intensity by means of a transdiode negative feedback circuit in the photomultiplier amplification system.

Most studies were made with crystals cut to expose the ac' or bc' faces. These faces eroded rapidly after polishing, reducing the degree of polarization and the transmitted intensity. Accurate long axis intensities were obtained from crystals cut with *ab* faces exposed and with naphthalene line absorption less than 0.3 O.D. units. The accuracy of short axis intensity measurements was limited by imperfect crystal polarization. Attempts to improve measurements by using index matching coatings were unsuccessful. The *p*-Xylene space group was reported to be P2 1/m with four molecules per unit cell,[8] but the complete crystal structure is not available. Mixed crystals were cut perpendicular to the cleavage plane with the extinction direction nearest to the fast growth axis in the exposed face. Under these conditions, the short naphthalene transition moment lies perpendicular to the cleavage plane, the long axis, parallel to it. No absorption occurs when the crystal is cut to expose the orthogonal direction.

III. RESULTS

In this section we will present the results which illustrate the nature of the interaction between the $^1B_{3u}$ and $^1B_{2u}$ states. By using different media, including vapor and various mixed crystals, the relative positions of the origins of these two states can be varied, and their interaction is thus altered. The same thing can be accomplished by isotopic substitution, since the zero point energies of the two states are different. We will also bring out evidence for the spectral features that are independent of the interaction, and try to show what the unperturbed spectra would be like. In a later section the data will be analyzed in more detail.

The absorption spectra of the vapor of three deuterium substituted naphthalenes in the region of the B_{2u} state are compared with that of the unsubstituted molecule in Figure 2. There are obvious similarities and a crude vibrational analysis shows that frequencies of 500, 1000 and 1380 cm^{-1} are present. These are close to known A_g modes in the ground and in the $^1B_{3u}$ states. The zero point energy shift can be noticed in these spectra with the origin bands of the two d_4 species lying between those of d_0 and d_8 (see Table I). The details of the band shapes for the four species differ from one to the other; we suppose that the different zero point shifts have caused differences to appear in the interaction between the B_{2u} state and B_{3u} overtones. Not

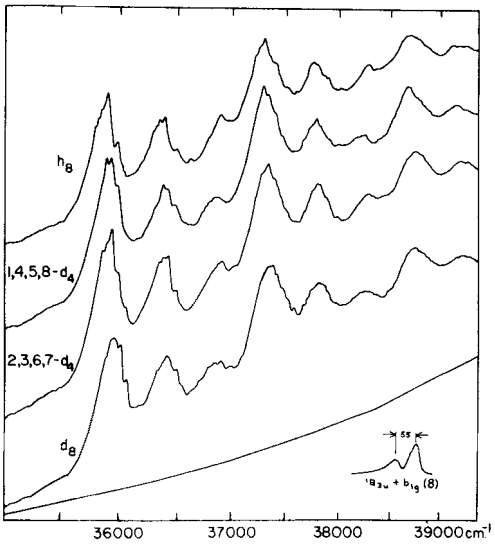

FIGURE 2 Gas phase absorption of the naphthalene $^1B_{2u} \leftarrow {}^1A_g$ system for the isotopes h_8, 1,4,5,8-d_4, 2,3,6,7-d_4, and d_8 at 298°K. The vertical scale is linear in log intensity. The 100% transmission baseline is recorded for the d_8 spectrum, all others are offset. Weak features below 37,500 cm^{-1} are reproducible.

The insert in the lower right hand corner is the $b_{1g}(8)$ line of the $^1B_{3u}$ system at 2.5 times the dispersion and 4 times the gain of the $^1B_{2u}$ spectra.

TABLE I

Solvent shifts, naphthalene-h_8

	$^1B_{3u}\bar{\lambda}$	$\bar{\lambda}_{vapor} - \bar{\lambda}$	$^1B_{2u}\bar{\lambda}^a$	$\bar{\lambda}_{vapor} - \bar{\lambda}$	$\bar{\lambda}_{^1B_{2u}} - \bar{\lambda}_{^1B_{3u}}{}^a$
Vapor	32,020.2	0.0 cm^{-1}	35,892	0	3872
n-pentane	31,747.4	272.8	34,550	1342 cm^{-1}	2803
Toluene (high energy)	31,733	287	34,600	1292	2867
Toluene (low energy)	31,505	515	34,400	1492	2895
Durene	31,556.2	464	34,550	1342	2994
p-xylene	31,285.9	734.3	33,730	2162	2474

Isotope Shifts

Durene	$^1B_{3u}\bar{\lambda}$	$\bar{\lambda} - \bar{\lambda}_{h\text{-}8}$	$^1B_{2u}\bar{\lambda}^a$	$\bar{\lambda}_{^1B_{2u}} - \bar{\lambda}_{^1B_{3u}}{}^a$
h-8	31,556.2	0.0 cm^{-1}	34,550	2994 cm^{-1}
1,4,5,8-*d*-4	31,596.5	40.3	34,560	2963
2,3,6,7-*d*-4	31,629.9	73.7	34,580	2950
d-8	31,671.0	114.8	34,640	2969

[a] Visual estimate of band center rather than the actual (0, 0) intensity centroid. Centroid estimates are about 250 cm^{-1} lower.

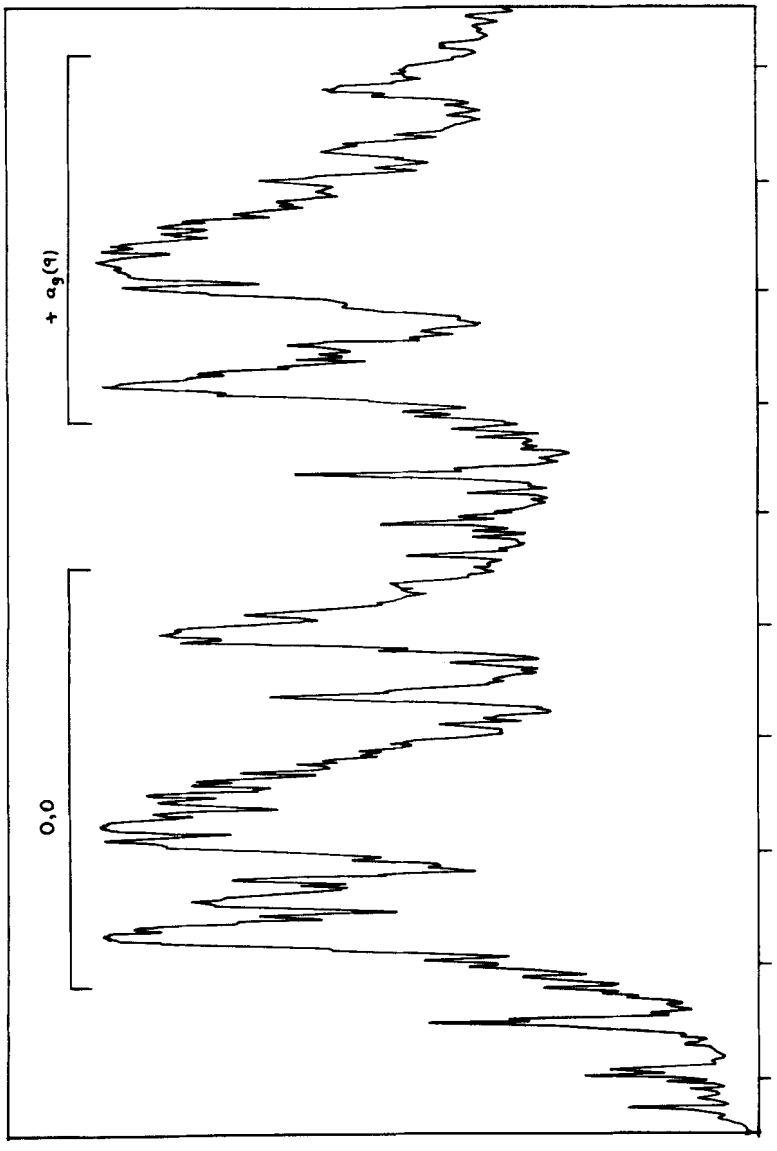

FIGURE 3 Photoelectric tracing of the origin and $+a_g(9)$ regions of h_8 naphthalene absorption in a durene crystal about 0.04 mole % in naphthalene at 2°K. Every distinct feature is reproducible. Many of the sharp weak features have widths less than 2 cm^{-1} at half height. The vertical scale is somewhat less than linear in optical density, compressed at high absorption by scattered light from the ab polarization. The line widths are instrument limited to 2 cm^{-1}. Brackets indicate the range of resonance vibronic interaction between the vibronic additions to the $^1B_{3u}$ system and the $^1B_{2u}$ origin and $+a_g(9)$ lines respectively.

much more can be done with such spectra, however, and we turn to the low temperature solid solution spectra.

Figure 3 shows a photoelectric tracing of the c'-polarized spectrum of naphthalene in durene at 2°K in the $^1B_{2u}$ origin region. The contrast with the vapor spectra is striking. It can now be seen that the fine structure suggested by the vapor spectra is actually resolved into bands having widths of only 2 cm^{-1}. The repetition of the origin band at 500 cm^{-1} (the $a_g(9)$ frequency) is seen in this figure. Notice also the repetition of the pattern from 34,350–34,460 in the region 34,850–34,960. The lower frequency set nominally belongs to the $^1B_{3u}$ state. The band width shown for the O, O region in Figure 3 is chosen to correspond to the bandwidth in the vapor, about 300 cm^{-1}. This width is what we have estimated to be the magnitude of the vibronic interaction between the two states.

The isotope shifts in the durene host crystal are the same as in the vapor. Figure 4, however, shows that the detailed structure of the bands is not at all similar from one isotopic molecule to another, a result suggested by the vapor spectra, but not shown as clearly there as in these crystal spectra. Such a complete change of structure cannot be ascribed to changes in low frequency

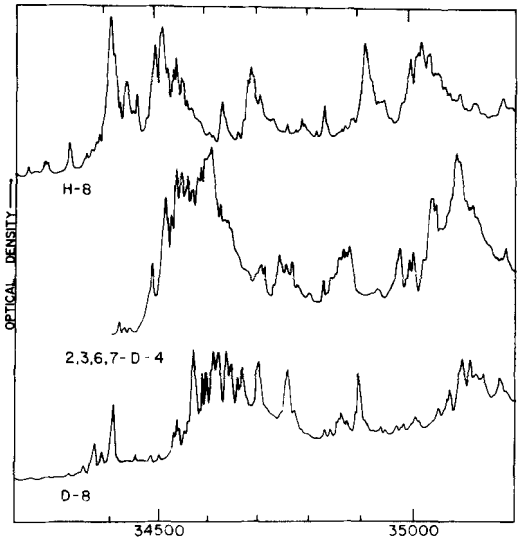

FIGURE 4 Comparison of the equivalent $^1B_{2u} \leftarrow {}^1A_g$ origin region absorption systems for h_8, 2,3,6,7-d_4, and d_8-naphthalene in durene at 2.2°K. The vertical scale is linear in log transmitted intensity. No baseline correction has been made. Crystals were about 10^{-4} mole fraction naphthalene and about 3 mm thick, oriented for c' axis polarization.

The 0,0 systems peak in the region 34,400–34,700 cm^{-1}; the $a_g(9)$ additions peak in the region 34,900 to 35,200 cm^{-1}. The large deuteration shift is evident. Also, the d_8 spectrum has more strongly coupled lines than the others.

modes of the different isotopically substituted molecules, but is most easily explained by the changed coincidences between the B_{2u}–B_{3u} energy differences and the B_{3u} vibrational overtones.

Other crystalline hosts produce a differential shift of the $^1B_{3u}$ and $^1B_{2u}$ origins similar to the isotope shifts. All of the origin shifts we have investigated are shown in Table I.

Although solid solutions of naphthalene in *n*-pentane and toluene showed fine structure, there were several sites for the naphthalene molecules; single crystals were not obtained either, so most of our work was done with durene and *p*-xylene as crystalline hosts. There is only one site for naphthalene in *p*-xylene and good single crystals were obtained. It was possible to separate cleanly the long axis spectrum from the short axis spectrum of naphthalene in p-xylene. This host transmits 300 cm^{-1} farther to the blue than durene, and shifts $^1B_{2u}$ 500 cm^{-1} closer to $^1B_{3u}$. Thus, we see a totally new set of coincidences in *p*-xylene.

The spectra of naphthalene in durene and in *p*-xylene in the interference region are shown together in Figure 5, and the corresponding spectra of *d*-8 are shown in Figure 6. In these figures the overtones of the $^1B_{3u}$ region in durene provide a first approximation to the unperturbed levels. The spectra in xylene are shifted (note different scales above and below) so that the $^1B_{3u}$ origins coincide. Thus the interaction region spectrum lies directly over the

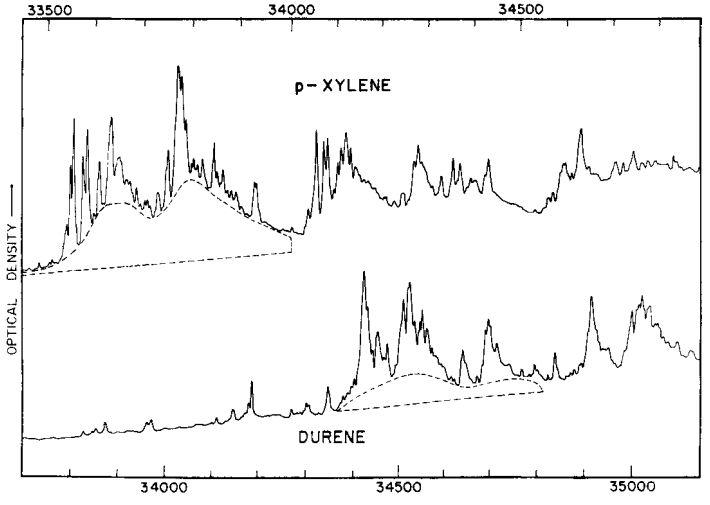

FIGURE 5 The short axis (*c'*)polarized absorption spectrum of h_8-naphthalene in *p*-xylene above the corresponding spectrum in durene, presented so that $^1B_{3u}$ origins are coincident. Dispersions are equivalent in wavelength, but not strictly comparable in energy. The vertical coordinate is linear in log intensity but is without correction. The areas of the origin systems attributed to the lattice excitation are enclosed by dotted contours.

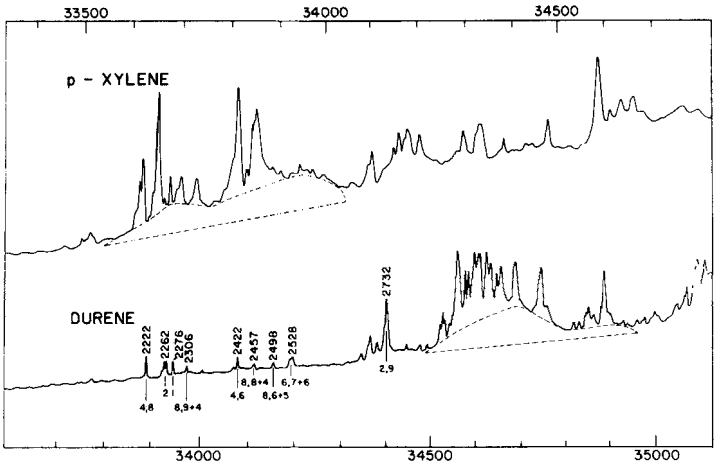

FIGURE 6 Logarithmic photoelectric tracing of the $^1B_{2u} \leftarrow {}^1A_g$ absorption system of naphthalene-d_8 in p-xylene above the corresponding tracing for durene, presented so that $^1B_{3u}$ origins are coincident. The dotted lines indicate the areas of phonon absorption in the origin bands. Discrete structure in p-xylene directly above the origin in durene is attributed to $^1B_{2u} + a_g(9)$. The absence of correlation between these spectra indicates that those vibrational additions to $^1B_{3u}$ which interact strongly with the $^1B_{2u}$ origin in durene do not interact with $^1B_{2u} + a_g(9)$ which is nearly isoenergetic with them in p-xylene.

In p-xylene the phononless components of the $^1B_{2u}$ origin have intensity 0.24, the phonons 0.76. Assignments for lines in durene are indicated by the b_{1g} mode number followed by the a_g excitations.

"unperturbed" spectrum in these figures. Certain resemblances can be found between the two when one realizes that a new state (the $^1B_{2u}$ origin) and some shifting of levels are present in the p-xylene spectra. A more careful analysis of these spectra will be presented in a later section.

It is clear that in order to understand the interaction between the $^1B_{3u}$ and $^1B_{2u}$ states, we will need to look at the spectra not just in the region of strong interaction shown in Figures 5 and 6, but will have to know the $^1B_{3u}$ spectra in detail in both host crystals. This will be necessary in order to estimate the unperturbed overtones lying in the region of strong interaction. In addition it is clear that the short-axis intensity in the $^1B_{3u}$ region comes from the same source as the complex structure of the $^1B_{2u}$ region and a complete theory of the coupling between the two states must explain both. Additional information on the nature of the interaction comes from the overtone region of the $^1B_{2u}$ state, as already seen in Figure 3.

Vibrational analyses of h-8 and d-8 in durene and in p-xylene were made for the $^1B_{3u}$ short and long axis spectra (8 tables in all).[1] Figures 7 and 8 show the short axis spectra and the major identifications for the two host crystals and isotopic molecules. The vibrational assignments are based on the ground state assignments of Freeman and Ross[9] and the work of McClure.[4]

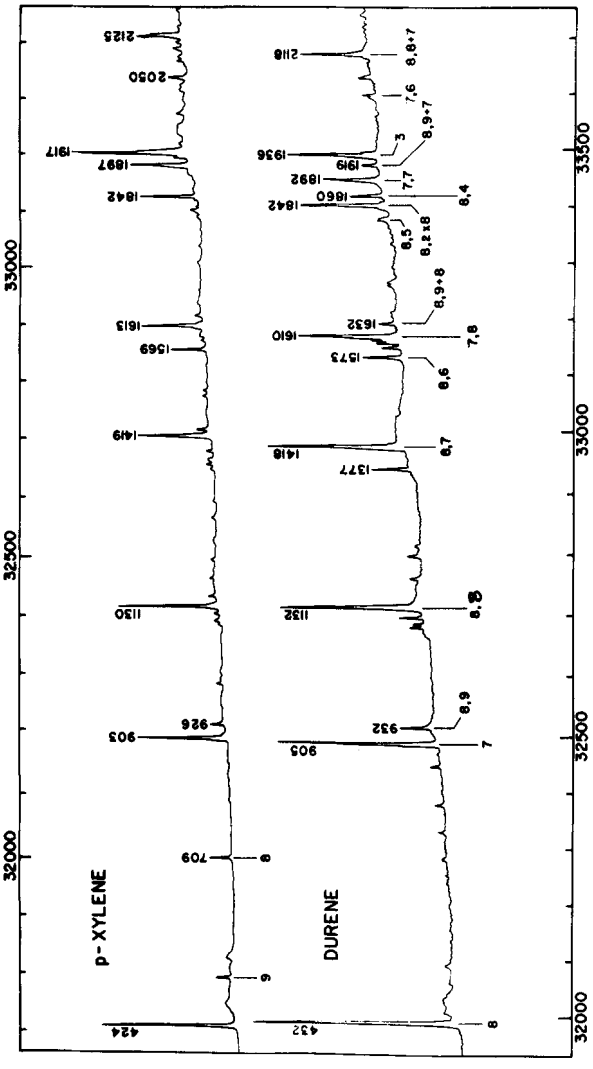

FIGURE 7 The short axis (c') polarized absorption spectra of h_8-naphthalene in *p*-xylene and durene hosts at 2.2°K. The vertical scale is linear in log intensity. Dispersions are linear in wavelength, but non-linear in the energy scale. No correction has been made for instrumental sensitivity as a function of energy. Polarization is not complete as evidenced by the presence of $a_g(8)$ in the *p*-*x* spectrum. Linewidths here are instrument limited. The crystals were about 3×10^{-4} mole fraction naphthalene.

Assignments appear below lines in the durene spectrum. The first number refers to the b_{1g} mode number, those following, to the a_g modes. Assignments below the *p*-xylene spectrum refer to the a_g modes which appear due to polarization contamination.

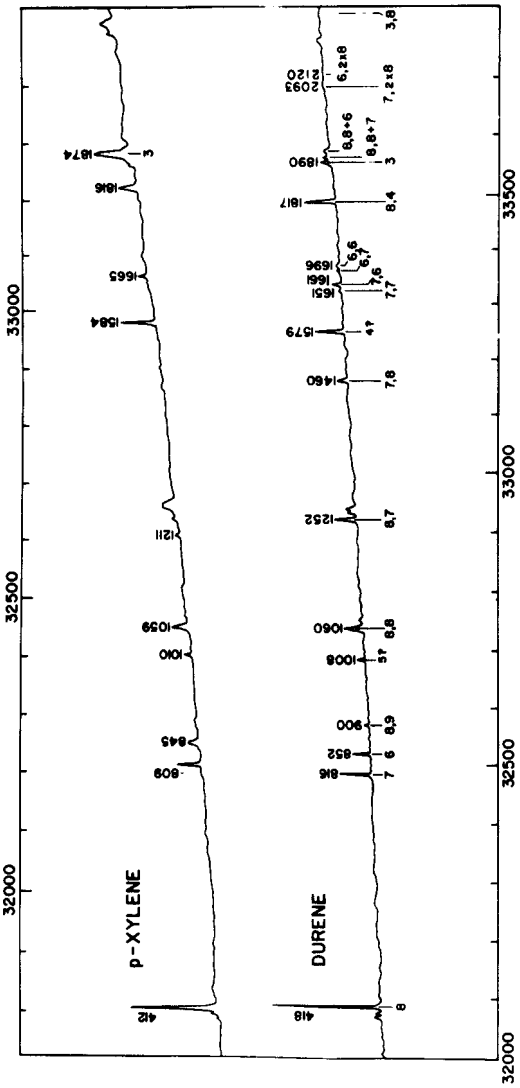

FIGURE 8 Logarithmic photoelectric tracing of the short axis polarized absorption system of d_8-naphthalene in *p*-xylene above the corresponding tracing for durene, presented so that $^1B_{3u}$ origins are coincident.

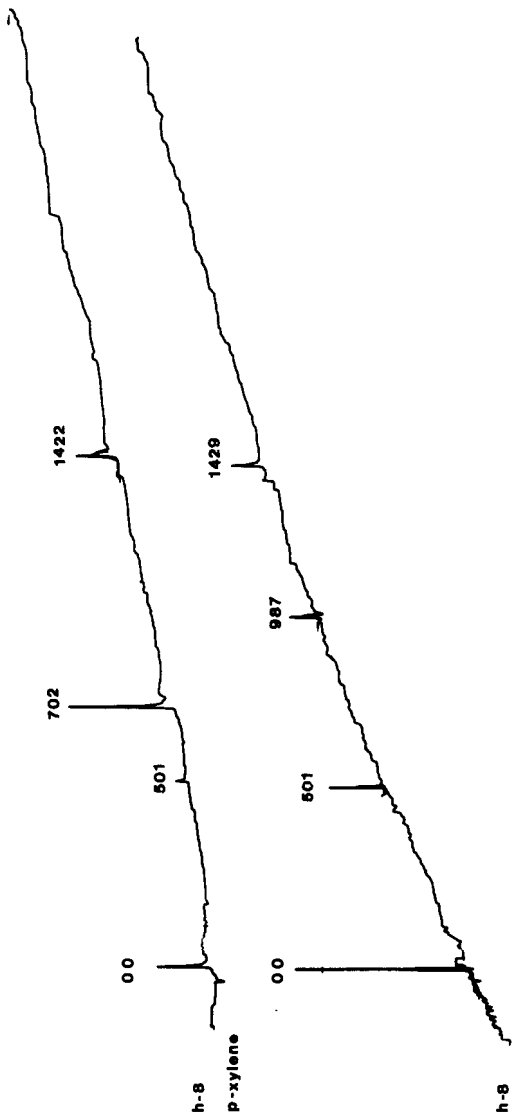

FIGURE 9 Microphotometer tracings of photographic spectra of naphthalene in *p*-xylene and in durene at 2°K in the $^1B_{3u}$ region, long axis polarized. Note the significant differences between the intensities of the same a_g mode addition in the two spectra.

TABLE II

Assignments of vibrations in the $^1B_{3u}$ state of naphthalene in durene[a]

	a_g			b_{1g}	
	h-8	*d*-8		*h*-8	*d*-8
1		(2272) 2262	1		2276(2302)
2		(2257)	2		2262(2257)
3	1516[b](1579)	(1553)	3	1611(1624)	1579(1575)
4	1429(1460)	1400(1381)	4	1377(1389)	(1330)
5	1385(1379)	1239(1293)	5	1232(1240)	1008(1030)
6	1143(1144)	845(866)	6		852(881)
7	987(1025)	836(835)	7	905(936)	816(784)
8	701(761)	642(692)	8	432(506)	418(490)
9	501(516)	482(493)			

[a] Most of these assignments are made by comparison with the ground state assignments.[9] Those for $a_g(5)$ in *d*-8 and for $b_{1g}(3)$, (4), and (5) in *h*-8 and *d*-8 are particularly speculative. They serve primarily to identify some recurring frequencies.

[b] This mode is unusually weak in absorption but must be important in the vibronic spectrum of $^1B_{3u}$ because of its prominence in combination with $b_{1g}(8)$.

The long axis spectrum gives the values of the a_g modes in the $^1B_{3u}$ state. There are nine such modes, and at least six can be assigned in *h*-8 and *d*-8, as shown in Table II for naphthalene in durene. Figure 9 compares the long axis spectra.

The long axis polarized spectrum is very weak, with oscillator strength $f = 4 \times 10^{-4}$ in durene and vapor absorption. The origin in durene and *p*-xylene is very sharp, and its true intensity measurement may be somewhat in error. From Figure 9 one can make estimates of the intensity of the a_g fundamentals relative to the origin. These values, of course, are the Franck–Condon factors from which geometry changes from the ground state might be inferred. There are some problems with this, however, as is seen by comparing the spectra in durene, xylene and in the vapor. The latter two have a similar intensity distribution of A_g modes in the long-axis spectrum, but this distribution is quite different in durene. It may be that coupling to the strongly allowed $^1A_g \rightarrow {}^1B_{3u}$ transition of durene near 50,000 cm^{-1} via dipole–dipole or other means can explain the intensity perturbations. The dipole moments of the naphthalene transitions are parallel to those of translationally equivalent durenes; however, although we do not know the *p*-xylene crystal structure, the shape of the *p*-xylene molecule is such that its $^1B_{3u} \rightarrow {}^1A_g$ transition should always be perpendicular to the long axis transition of naphthalene. In this case the transitions on the two molecules would remain uncoupled, and the spectrum in *p*-xylene would be less perturbed. This appears to agree with the observations. A calculation of this coupling supports this conclusion.[1]

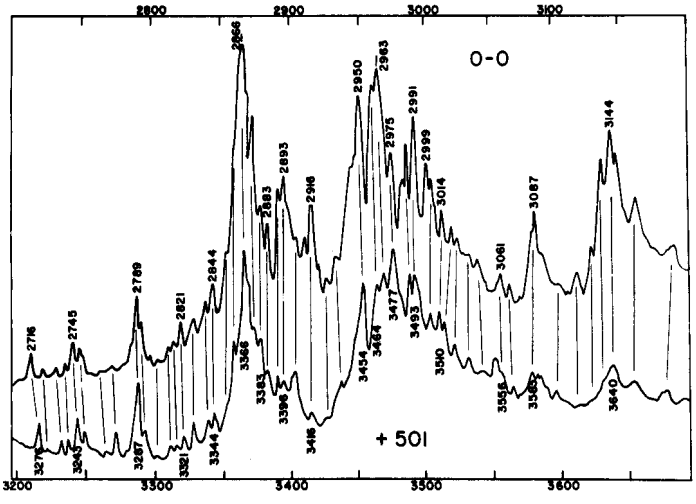

FIGURE 10 Direct comparison of band systems of the $^1B_{2u} \leftarrow {}^1A_g$ origin (top) and the $^1B_{2u} + A_u(9) \leftarrow {}^1A_g$ transitions in the durene host at 2°K. One-to-one correspondence of features is indicated by the vertical lines. The lower trace is offset by 500 cm^{-1} to lower energy. Both are taken from a photoelectric tracing that is linear in log intensity. This spectrum is a good example of the complexity in this region and shows the optical resolution available in these systems.

If it were not for the vibronic interference between $^1B_{3u}$ and $^1B_{2u}$, the spectrum due to the $^1B_{2u}$ state would apparently be quite simple. This is shown in Figures 10 and 11, where it is seen that the complex origin structure is repeated almost exactly at frequency intervals corresponding to the a_g modes. Figure 10 shows the correlation for naphthalene in durene, and it can be compared with Figure 3 in which the resolution is somewhat greater. Figure 11 compares three overtones of naphthalene in *p*-xylene with the B_{2u} origin region. Here again, many similarities are evident.

DISCUSSION

The remarkable interpretation given by Langhoff and Robinson[2] (LR) to the spectra we have just described would seem to make any further discussion superfluous. They were able to reduce these complex perturbed spectra to zero order unperturbed spectra, and thereby to interpret them in detail. Their results amounted to the removal of the perturbation between $^1B_{2u}$ and the $^1B_{3u} + b_{1g} + na_g$ overtones in the strongly interacting region. Once this perturbation is removed, the unperturbed level positions can be analyzed by the traditional spectroscopic methods of adding up vibrational quanta, and the levels are then assigned. These allow the continuation of the spectra shown in Figures 7 and 8 on through the beginning of the $^1B_{2u}$ spectrum. Further-

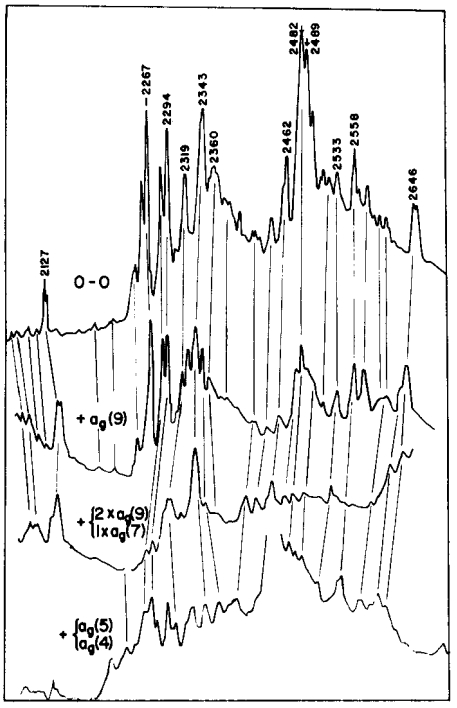

FIGURE 11 Direct comparison of band systems of the $^1B_{2u} \leftarrow {}^1A_g$ origin (top), the $^1B_{2u} + A_g(9) \leftarrow {}^1A_g$, the $^1B_{2u} + A_g(7) \leftarrow {}^1A_g$, and the $^1B_{2u} + A_g(4) \leftarrow {}^1A_g$ transitions in the *p*-xylene host at 2.2°K. More features of the $^1B_{2u}$ are observable in *p*-xylene than in durene because the electronic transition is at lower energy. Correlation between features of the appropriately offset transitions are indicated by the vertical lines. Energy dispersion decreases in the higher energy systems so the correlating lines tend to converge. The intense feature in the $A_g(4)$ band seems to correspond to a prominent feature of the durene spectrum and has no counterpart in the lower energy *p*-xylene spectrum.

more, the unperturbed origin of $^1B_{2u}$ is located and the interaction parameters are found.

The work of LR is based on the use of a single perturbing level and its mixing with secondary levels. This treatment takes account of the real linewidths associated with continua. Their method would apply to any spectrum. Yet there are aspects of this work as it has been applied to naphthalene which make it incomplete. First, the coupling parameters for each intensified line are left unexplained. A component of each such coupling parameter must be a Franck–Condon factor of the type $\langle \chi_3^1 | Q_{b_{1g}}^i | \chi_g^0 \rangle$ multiplied by Franck–Condon overlap factors for the other modes. Here $Q_{b_{1g}}^i$ is a displacement in the *i*th type of b_{1g} mode; χ_3^1 is a one quantum wave-function of a b_{1g}(i) mode in $^1B_{3u}$, and χ_2^0 is the zero quantum b_{1g} wavefunction in $^1A_{gu}$. These factors depend upon the molecular geometry and force field. Second, since the

transition moment to the $^1B_{2u}$ state is distributed over several of its vibrational substates, the intensity borrowing in the region of the $^1B_{3u}$ state cannot be obtained correctly by assuming only one intensity source. A complete theory would be able to handle the entire vibronic coupling problem. Thirdly, the treatment of L.R. neglects the relatively strong interactions between $^1B_{2u}$ and the low energy vibronic levels of $^1B_{3u}$.

These objections are not fundamental to the L.R. treatment; however, they were met in the original treatment of this problem by Wessel[1] which was based on Herzberg–Teller theory. This treatment was partially described by L. R., but a fuller description and the results will be given here.

The problem is very complex, and therefore some approximations were made and the calculations were done in several stages. First the intensity of the short axis B_{3u} spectrum was worked out. This could be done using perturbation theory, and it was possible to include not only the $^1B_{2u}$ O, O intensity source, but also the a_g additions to it. An important complication in doing this is that the $^1A_g \rightarrow {}^1B_{2u}$ transition moments have definite phase relations with the a_g vibrational displacements which are needed to map the B_{2u} geometry onto that of B_{3u}. These interference effects are clearly evident in the $^1B_{3u}$ spectrum. The results give the correct coupling constants to all the levels of the B_{3u} spectrum in durene up to 2500 cm^{-1} from the origin in terms of the vibronic coupling parameters for the active b_{1g} modes.

In the second stage, the resonance region is treated, but only one intensity source is used, the $^1B_{2u}$ origin level. This is justified because the intensified lines all lie within 200 cm^{-1} of the $^1B_{2u}$ level, while other intensity sources are relatively much farther away.

a. Calculation of the intensity of the ^1A_g-$^1B_{3u}$ short-axis spectrum

Intensities of the short axis lines of less than resonant energy are of great importance to calculation of resonance interactions because their strengths are derived from the $^1B_{2u} \leftarrow {}^1A_g$ transition by vibronic coupling. Energy perturbations are less useful as a source of coupling information because the zero order energies are unknown and shifts far from the resonance region are slight: whereas all zero order intensities are zero, except that of the $^1B_{2u}$ donor state, and intensification is often appreciable. First order perturbation theory allows coupling strengths to be derived from the intensity of the lines when their distance from the $^1B_{2u}$ origin is large relative to the interaction energy.

Intensities of lines in progressions built upon single b_{1g} excitations should be related to the coupling strength of the b_{1g} mode and to the overlap factors appearing in terms connecting the $^1B_{3u}$ levels with the $^1B_{2u}$ transition moment sources. The conventional first order Herzberg–Teller treatment gives

the following vibronic transition intensity

$$I(^1B_{3u}, 1 \times b_{1g}, n \times a_g^{(3)})$$
$$= \Bigg[\sum_{n'} \Bigg\{ \left\langle {}^1B_{2u} \left| \frac{\partial H}{\partial Q_{b_{1g}}} \right| {}^1B_{3u} \right\rangle \langle 0 \times b_{1g}^{(2)} | \delta Q_{b_{1g}} | 1 \times {}^{b(3)}_{1g} \rangle$$
$$\times \langle n' \times a_g^{(2)} | n \times a_g^{(3)} \rangle \times \langle | \rangle' \times \vec{M}(^1B_{2u}, n' \times a_g^{(2)})$$
$$\times [E(^1B_{3u}, 1 \times b_{1g}, n \times a_g) - E(^1B_{2u}, 0 \times b_{1g}, n' \times a_g)]^{-1} \Bigg\} \Bigg]^2 \quad (1)$$

where $\langle | \rangle'$ is the overlap for the modes that do not change excitation. This equation specifies that the a_g additions to b_{1g} excitation in the $^1B_{3u}$ spectrum obtain intensity from a sum over all borrowed $^1B_{2u}$ transition moments, denoted by $\vec{M}$. Each contribution from first order theory consists of a product of factors giving the electronic coupling provided by the b_{1g} vibration, the vibrational displacement of this mode between the $^1B_{2u}$ and $^1B_{3u}$ states, the overlap of the a_g mode that changes excitation, the overlaps of all the modes retaining original excitation, and the signed vector transition moment $\vec{M}$ for the donor a_g excitation of the $^1B_{2u}$ state. Each term must be divided by the appropriate energy denominator. Intensity is obtained from the square of the signed vector sum over all $^1B_{2u}$ intensity sources. The moments $\vec{M}$ have phases determined by the direction of nuclear displacement between ground and excited states along the mode excited. The a_g overlap factors have phases appropriate to $^1B_{2u} - {}^1B_{3u}$ equilibrium displacement.[10] Phasing options are illustrated in Figure 12 and enumerated in Table III.

This treatment assumes the normal coordinate space does not change greatly between the $^1B_{3u}$ and $^1B_{2u}$ states. The same a_g modes are important in both states. The moderate intensity of a_g additions to the vibronic false origins indicate that Franck–Condon displacement factors† between the two states must be about 1.5 or less.

b. Phasing options and movement interference

The line strengths of a_g additions relative to the pure b_{1g} false origins will be given by Eq. 1 for the low energy region. If the displacement coordinates were near zero, the diagonal coupling would cause the induced spectrum to reflect the $^1B_{2u} + a_g$ addition spectrum. In calculations that have been made for intensity ratios, assuming various displacement coordinates along $a_g(9)$ and $a_g(4)$, severe intensity reductions occur at displacements of order 0.5,

† The displacement factor δ is related to the intensity ratio by $\delta^n/(2^n n!)^{1/2} = (I_{on}/I_{oo})^{1/2}$ when the mode frequency does not change appreciably.

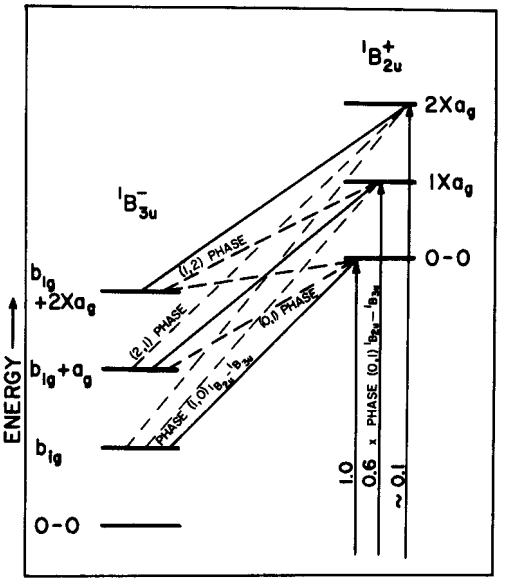

FIGURE 12 Phasing options for $^1B_{2u} - {}^1B_{3u}$ coupling. Vibronically induced levels of the $^1B_{3u}$ system appear on the left with lines connecting along paths of vibronic interaction to the $^1B_{2u}$ intensity sources that appear on the right. The strong coupling diagonal in a_g excitation is indicated by the solid diagonal lines. The intensities of the moment sources are entered along the moment transitions.

indicating that phase cancellation is important at small equilibrium displacement if moment sources of appropriate phase are present. Nearly complete cancellation is achieved in $a_g(9)$ plus $b_{1g}(8)$ for displacements 0.6 and 1.05 according to moment calculations that have been recorded in Figure 13. The behavior for out-of-phase coupling in $a_g(4)$, shown in Figure 14, indicates displacement 0.5 or 0.95 must occur along this mode. Two displacement values are consistent with each observed intensity because intensity is quadratic in the displacement. A decision as to which value is to be chosen was made on the basis of mode displacement calculations using bond order changes between ground and excited states.[1]

These are the only a_g modes with important $^1B_{2u}$ moment sources other than the 0, 0. Moment interference will be impossible for the remaining modes which obtain intensity primarily by off-diagonal coupling to the origin.

c. The resonance region $^1B_{2u} \leftarrow {}^1A_{\parallel}$ Transition energies and intensities

The interaction patterns should follow from diagonalization of the full vibronic Hamiltonian in a basis consisting of the zero order Born–Oppenheimer product states for the $^1B_{2u}$ totally symmetric vibrational levels, including the

TABLE III

Phasing options

a_g Excitation in $^1B_{3u}$ ↓	$M(^1B_{3u}, 1 \times b_{1g}, n' \times a_g \leftarrow {}^1A_g, 0 \times b_{1g}, 0 \times a_g)$ $= \langle \psi^{elec}(^1B_{2u}) \vert H^{elec}(\text{Vibronic}) \vert \psi^{elec}(^1B_{3u}) \rangle \times \langle 0 \times b_{1g} \vert \delta Q_{b_{1g}} \vert 1 \times b_{1g} \rangle$ $\times M^0(^1B_{2u} \leftarrow {}^1A_g) \times a_g$ Excitation in $^1B_{2u}$ →
$n' = 0$	$\frac{\langle 0_{B_{2u}} \vert 0_{B_{3u}} \rangle \langle 0_{B_{2u}} \vert 0_{A_g} \rangle}{\Delta E(^1B_{2u} - {}^1B_{3u}) - E(b_{1g})} + \frac{\langle 1_{B_{2u}} \vert 0_{B_{3u}} \rangle \langle 1_{B_{2u}} \vert 0_{A_g} \rangle}{\Delta E - E(b_{1g}) + E(a_g)} + \frac{\langle 2_{B_{2u}} \vert 0_{B_{3u}} \rangle \langle 2_{B_{2u}} \vert 0_{A_g} \rangle}{\Delta E - E(b_{1g}) + 2E(a_g)}$
$n' = 1$	$\frac{\langle 0_2 \vert 1_3 \rangle \langle 0_2 \vert 0_g \rangle}{\Delta E - E(b_{1g}) - E(a_g)} + \frac{\langle 1_2 \vert 1_3 \rangle \langle 1_2 \vert 0_g \rangle}{\Delta E - E(b_{1g})} + \frac{\langle 2_2 \vert 1_3 \rangle \langle 2_2 \vert 0_g \rangle}{\Delta E - E(b_{1g}) + E(a_g)}$
$n' = 2$	$\frac{\langle 0_2 \vert 2_3 \rangle \langle 0_2 \vert 0_g \rangle}{\Delta E - E(b_{1g}) - 2E(a_g)} + \frac{\langle 1_2 \vert 2_3 \rangle \langle 1_2 \vert 0_g \rangle}{\Delta E - E(b_{1g}) - E(a_g)} + \frac{\langle 2_2 \vert 2_3 \rangle \langle 2_2 \vert 0_g \rangle}{\Delta E - E(b_{1g})}$

$\langle 1_2 \vert 0_3 \rangle = -\langle 0_2 \vert 1_3 \rangle$; $\langle 1_2 \vert 0_g \rangle = -\langle 0_2 \vert 1_g \rangle$

Four phase choices are possible:

$\langle 1_2 \vert 0_3 \rangle = +\langle 1_2 \vert 0_g \rangle = +$ $\qquad$ $\langle 1_2 \vert 0_3 \rangle = +\langle 1_2 \vert 0_g \rangle = -$

Moment borrowing terms

$n' = 0$	+ + +	+ − +
→ 1	− + +	− − +
2	+ − +	+ + +

$\langle 1_2 \vert 0_3 \rangle = -\langle 1_2 \vert 0_g \rangle = +$ $\qquad$ $\langle 1_2 \vert 0_3 \rangle = -\langle 1_2 \vert 0_g \rangle = -$

$n' = 0$	+ − +	→ + + +
1	+ + −	+ − −
2	+ + +	+ − +

The arrow denotes phase choices consistent with $a_g(9)$ and $a_g(4)$ additions to $b_{1g}(8)$.

[a] The relative signs of the term in Eq. 1, shown at the top of the table, have to be determined. The moment sources are $M(^1B_{2u} + {}^1A_u) \times a_g$ excitations in $^1B_{2u}$, whose F. C. overlap is $(nB_{2u} \vert 0_{A_{1g}})$ and can be positive or negative. The perturbed state has an a_g overlap factor $(nB_{2u} \vert n'B_{3u})$. The possible relative signs of the products of these factors for different values of n and n' are shown in the boxes. The important $a_g(9)$ and $a_g(4)$ modes probably have the phase relations shown, as determined by the experimental intensities and mode displacement calculations.

zero point level, and the vibronic additions to the $^1B_{3u}$ level of B_{2u} overall symmetry. If the coupling matrix elements for interaction between the $^1B_{2u}$ and $^1B_{3u}$ states and the zero order energy levels could be estimated, the diagonalization would lead to the observed spectrum. This calculation would prove that the complex resonance structure derived from vibronic level interference and it would supply the correct $^1B_{3u}(1)$ wave-functions. Complications such as the distribution of interaction between phononless and phonon (lattice) lines and estimation of coupling pathways complicate application of such techniques but certain approximations and observations about coupling matrix elements have made the interaction calculation possible.

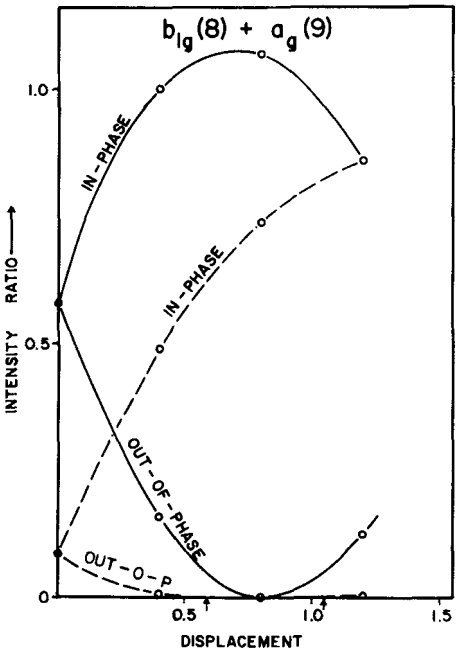

FIGURE 13 Intensity of the $a_g(9)$ addition to the $b_{1g}(8)$ relative to the pure $b_{1g}(8)$ in the $^1B_{3u}$ spectrum predicted by first order perturbation theory as a function of the nuclear displacement coordinate along $a_g(9)$ connecting $^1B_{2u}$ and $^1B_{3u}$ states. Moment sources 2740, 3240 and 4140 cm^{-1} above the $^1B_{3u}$ origin with moments in the ratio 1.0, 0.8 and 1.2 were assumed. The solid upper curve is for additive phasing between the borrowed $^1B_{2u}$ origin moment and the borrowed $^1B_{2u} + a_g(9)$ moment. The solid lower curve is for destructive moment phasing. Dashed curves are for two-quantum excitations in $a_g(9)$. Calculations for naphthalene-d_8 are nearly identical.

The arrows along the abscissa indicate the two displacements consistent with the observed intensity ratio, 0.05 (which implies out-of-phase interaction).

In the region of resonance, it may be justified to take only one intensity source, the $^1B_{2u}$ origin and ignore the a_g additions. The Hamiltonian would then have the simple form:

$$H = \begin{bmatrix} H(1,1) & H(1,2) & H(1,3) & \cdots & H(1,n) \\ H(1,2) & H(2,2) & & & \\ H(1,3) & & H(3,3) & & \bigcirc \\ \vdots & & & \ddots & \\ H(1,n) & & \bigcirc & & H(n,n) \end{bmatrix} \tag{2}$$

where $H(1,1)$ is the zero order $^1B_{2u}$ origin energy. $H(n,n)$ are the zero order $^1B_{3u}$ levels of $^1B_{2u}$ vibronic symmetry, and $H(1,n)$ are the off-diagonal vibronic interaction terms.

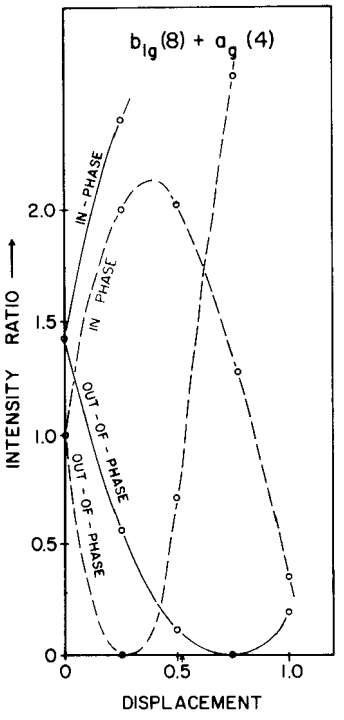

FIGURE 14 Intensity of the $a_g(4)$ addition to the $b_{1g}(8)$ relative to the pure $b_{1g}(8)$ in the $^1B_{3u}$ spectrum predicted by first order perturbation theory. The observed intensity is 0.09.

Calculation of the intensities and positions of the lines in the region assumed to be the $^1B_{2u}$ origin requires estimation of the intensity and position of the $^1B_{2u}$ zero order origin ($H(1, 1)$ in Eq. 2). Fortunately this level bears all the short axis intensity in the resonance region so that interaction with the $^1B_{3u}$ manifold merely redistributes $^1B_{2u}$ origin intensity, preserving the center of gravity. Visual estimation of the centroid for the first band system of h-8 naphthalene in durene placed this level 3000 cm^{-1} above the $^1B_{3u}$ origin. The actual transition energy must be estimated from the centroid of intensity of all lines that derive from the origin. Line intensities have to be obtained for this calculation. The 300 cm^{-1} band width of the origin system causes considerable overlap with the $^1B_{2u} + a_g(9)$ band 500 cm^{-1} to higher energy. Arbitrary assignments of parentage for lines occurring between these bands were necessary.

It was not clear initially whether the lattice modes would have to be included in the centroid calculation. The lattice structure in the resonance region is not distinct from the phononless line structure because the lattice intensity associated with each interacting vibrational level starts about 20 cm^{-1} above

the phononless line, extending 50 cm^{-1} to higher energy with a smooth contour. Therefore severe overlapping of lattice bands occurs in the resonance region. The proportion of zero order $^1B_{2u}0, 0$ intensity associated with lattice excitation was estimated first for the *p*-xylene spectra (in which phononless line overlap is minimal: most sharp lines are separated by several linewidths). It appears reasonable to attribute the intensity underlying the sharp structure to the composite overlapping lattice components. A baseline was constructed in order to separate sharp lines from the composite lattice absorption band. The resultant separation shown in Figure 5 gives the phononless structure an intensity of 0.22 and the lattice intensity 0.78, close to the intensity distribution in the low energy short axis spectrum: 0.35 for the 424 cm line, and 0.65 in the associated lattice shown in Figure 15. The similarity of intensity distribution in $^1B_{2u}$ and $^1B_{3u}$ regions supports the assumed separation into line and lattice sources of vibronic intensity.

Therefore the $^1B_{2u}$ origin band centroid calculation was obtained by summing the products of line intensity times line energy over all the lines attributed to the $^1B_{2u}$ origin system. There are few levels built upon the $^1B_{3u}$ origin occurring in the region 2600 to 3000 cm^{-1} above the $^1B_{3u}$ origin that have strong coupling to the $^1B_{2u}$ origin. Most of the $^1B_{3u}$ vibrational additions in this region share intensity from the $^1B_{2u}$ origin and $a_g(9)$ addition. Therefore an arbitrary cut-off was imposed at 2640 cm^{-1} for *h*-8 naphthalene

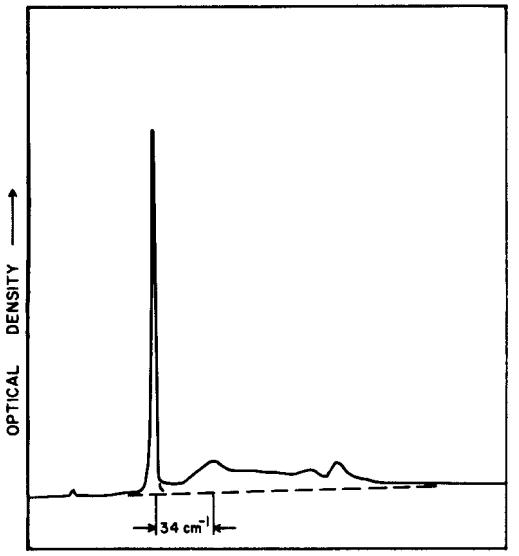

FIGURE 15 The $^1B_{3u}$ origin in *p*-xylene at 2°K with 2 cm^{-1} resolution. Scattered intensity was negligible so the tracing should be logarithmic.

in *p*-xylene and at 3200 cm^{-1} for *h*-8 in durene. The former choice seems moderately compelling because the last line in the origin band group is clearly out of the $a_g(9)$ addition region. The low energy lines of the $^1B_{3u}$ short axis spectrum are very intense so they contribute substantially to the centroid position. In fact, although the origin band center appears near 2400 cm^{-1} in *p*-xylene and 3000 cm^{-1} in durene, the calculations place the centroids at 2220 and 2740 cm^{-1} above the $^1B_{3u}$ origin, respectively. The low energy lines shift the calculated centroid downward because they are far below the apparent resonance. The ideal centroid calculation would be the diagonalization itself. When the zero order $^1B_{2u}$ position is estimated correctly, the intensity distribution among the resonant levels should match the observed spectrum. The $^1B_{2u}$ position in *p*-xylene that yields the best diagonalization is 2190 cm^{-1} above the $^1B_{3u}$ origin. This is in satisfactory agreement with the value 2220. Estimates for the *d*-8 centroids are within 20 cm^{-1} of the *h*-8 values. For *d*-8 in *p*-xylene, the diagonalization best fits the spectrum with $^1B_{2u}$ 0, 0 again at 2190 cm^{-1}. These large shifts of the centroid from the apparent band center are partly artificial because the low energy lines get part of this intensity from $B_{2u} + a_g$ additions. But the centroid position calculated without these additions is a check on the diagonalization which includes only the B_{2u} origin source.

d. The spectrum in durene as a guide to resonance in *p*-xylene

At this point, we could extrapolate the $^1B_{3u}$ short-axis spectrum into the resonance region, to provide the diagonal elements of Eq. 2, including the centroid of $^1B_{2u}$ which we have just located. The off-diagonal elements are not known accurately enough, however, because we do not have good information on the a_g overlap factors. Therefore we tried another approach.

Lines of naphthalene in durene near the $^1B_{2u}$ resonance energy in the *p*-xylene host have energy denominators favoring coupling to the $^1B_{2u}$ origin system. Only those with very strong diagonal coupling to other moment sources will have interference contributions. The origin in durene is 550 cm^{-1} higher relative to the $^1B_{3u}$ than in *p*-xylene so first order perturbation theory will apply to lines in durene that are in the region of resonance in *p*-xylene.

Therefore the durene spectrum has been used as a guide in estimating coupling for the $^1B_{3u}$ levels of B_{2u} vibronic symmetry at resonance with the $^1B_{2u}$ in *p*-xylene. The resonance region absorption of the $^1B_{2u}$ 0, 0 in *p*-xylene is compared with the iso-energetic region in durene in Figures 16 and 17. If several intensity sources were important in this region, it would not be possible to transfer the coupling matrix elements directly to the xylene spectrum unless the importance of each path in terms of the off-diagonal overlap factors involved were known beforehand.

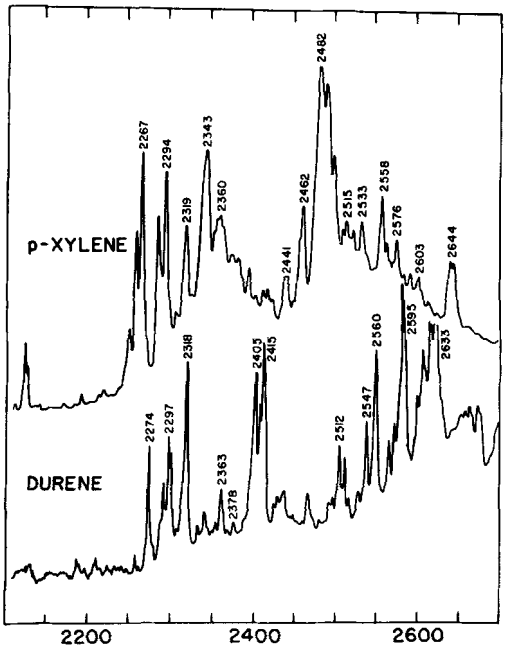

FIGURE 16 Naphthalene-h_8 $^1B_{2u}$ origin in *p*-xylene and the isoenergetic region in durene. The naphthalene-h_8 $^1B_{2u}$ origin in *p*-xylene appears above the region in durene which has equivalent separation from the $^1B_{3u}$ origin. The optical density scale in durene is expanded by a factor of 12 so that the structure in this region which is far from $^1B_{2u}$ resonance will be clear.

The intent of the diagonalization calculation is to take the weakly perturbed lines in the durene spectrum, interact them with a single $^1B_{2u}$ origin level positioned at the center of the $^1B_{2u}$ origin band in *p*-xylene, and thereby generate the *p*-xylene spectrum.

Before going into specific detail we outline the steps of this treatment:

1) Apparent vibronic interaction matrix elements are estimated from the durene spectrum assuming all intensity is from the $^1B_{2u}$ origin. The first order perturbation theory gives the result

$$H(1, n) = I(n)^{1/2}\Delta E \tag{3}$$

where ΔE is the separation between the $^1B_{3u}$ level and the $^1B_{2u}$ origin.

2) The zero order $^1B_{3u}$ energies are obtained by correcting the durene frequencies to zero order by subtracting the first order perturbation energy. Thus,

$$H(n, n) = E(\text{Durene}) + \frac{H(1, n)^2}{\Delta E} \tag{4}$$

3) The resultant interaction matrix is diagonalized. The energies and intensities differ seriously from the observed spectrum.

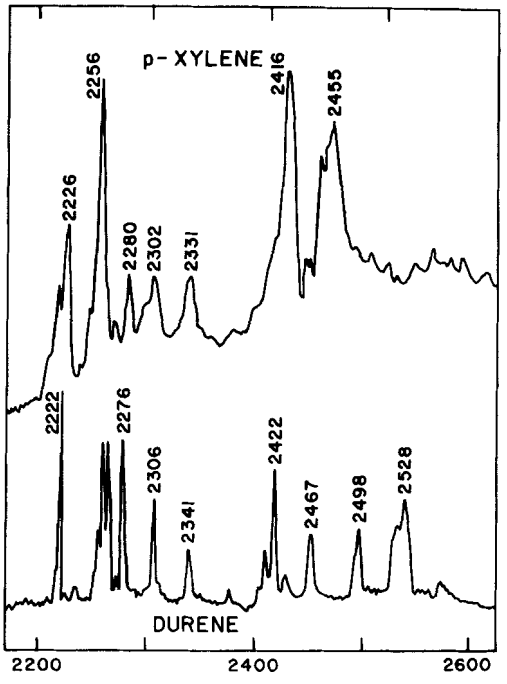

FIGURE 17 Naphthalene-d_8 $^1B_{2u}$ origin in *p*-xylene and the isoenergetic region in durene. The naphthalene-d_8 $^1B_{2u}$ origin in *p*-xylene appears above the region in durene which has equivalent separation from $^1B_{3u}$ origin. The optical density scale in durene is expanded by a factor of 4.

4) The $^1B_{2u}$ zero order component $H(1, 1)$ is moved until diagonalization yields a reasonable intensity distribution.

5) Energy and intensity Jacobians are used to adjust each matrix element and the diagonalization is repeated. The process is iterated until the observed spectrum is fitted.

6) The diagonal elements of the matrix before the last diagonalization give the zero order energies, the off-diagonal elements give the vibronic coupling interactions.

Before showing the results of this program, several special topics related to the matrix, Eq. 2, will be discussed.

1. *Contributions from a_g additions to the $^1B_{2u}$ origin* Estimates by equation 3 are frequently unsatisfactory. In the early stages of this work coupling between $^1B_{3u}$ short axis lines and the $^1B_{2u}$ levels was assumed to be nearly diagonal in the a_g vibrations. Lines well below the origin would then have

intensity contributions from levels above the $^1B_{2u}$ origin and use of Eq. 3 would overestimate coupling. It became apparent that these estimates were too small to generate the observed spectrum. This problem was not resolved until the moment interference model, equation 1, had been developed. It was then apparent that most intense excitations have predominate coupling to the origin. Therefore Eq. 3 remains useful provided that allowance is made for several lines which have unusually low intensity due to moment interference.

2. *Off-diagonal coupling to $^1B_{2u}$ lattice intensity* Coupling to $^1B_{2u}$ lattice transition moment sources remains as an unsolved problem. The interaction estimates by equation 3 in durene are relatively insensitive to off-diagonal interaction between the phononless $^1B_{3u}$ lines and the $^1B_{2u}$ origin lattice states because the energy denominator, ΔE, for this interaction is only 50 cm^{-1} larger than that for the diagonal phononless interaction. In the *p*-xylene resonance region these same $^1B_{3u}$ levels are embedded in the $^1B_{2u}$ origin lattice "continuum". The energy denominators for off-diagonal coupling from the $^1B_{3u}$ phononless levels to the $^1B_{2u}$ lattice states relative to the diagonal coupling to the phononless $^1B_{2u}$ origin will be very sensitive to the line positions. Whenever a $^1B_{3u}$ phononless component occurs 50 to 150 cm^{-1} above the zero order $^1B_{3u}$ phononless component, it should interact far more with the lattice than otherwise. This effect may be responsible for the pronounced decrease in density of sharp strong features 50 to 150 cm^{-1} above the strongest components of the *h*-8 origin resonance spectra (at 2482 and 2455 cm^{-1} respectively). They may in fact be affected by antiresonance with the phonon continuum.[11]

3. *Second order interaction and intensification of weakly coupled lines* Several observations about matrix diagonalization behavior for Hamiltonians with all off-diagonal terms of the form $H(1, n)$ and $H(n, 1)$ simplify the interpretation. If two of the zero order levels of the vibronic spectrum, m and n, are close together, and $\langle n|H'|1\rangle$ is large, $\langle m|H'|1\rangle$ small, the eigenfunctions corresponding to the terms m and n will both contain large components of state 1, which represents the $^1B_{2u}$ level. This is actually a case of second order coupling between a strong and a weak line through the $^1B_{2u}$ intermediate state. The energy denominators for the intensity of the weak line are $(E_m - E_{1_{B2u}}) \times (E_m - E_n)$ where the last term is very small when the lines are close together. Therefore, weak lines can steal from nearby strong ones even though the $^1B_{2u}$ is distant. If lines intense after interaction fall near slightly perturbed weak ones, the weak gain abnormal intensity. Striking examples of this phenomena occur in the *h*-8 spectrum in *p*-xylene shown in Figure 16. There seem to be subgroups of two and three components near 2294 and

2267 cm^{-1} above the origin, and at 2489 and 2641 cm^{-1}. There are not enough strong coupling combinations to allow a one-to-one correspondence between strong coupling lines in durene and strong features of the $^1B_{3u}$ spectrum in xylene (see Figure 16). For example only one line, 2274, occurs in durene (weakly) near the 2267 group of *p*-xylene. Therefore local intensification follows the strongly interacting components, resulting in complex band patterns. No attempt has been made to predict the fine structures of these systems because the inhomogeneous solvent shifts alone must be so large as to leave uncertainties in zero order diagonal matrix elements far greater than the 2 cm^{-1} required for good fits to the data. This phenomenon makes it possible to simplify the initial and final spectra for purposes of simplifying the matrix diagonalization.

e. Diagonalization results and comparison of the *p*-xylene resonance region with the isoenergetic region in durene

The diagonalization calculations have been made and refined. The initial estimates to zero order energies and interactions are listed in columns 5 and 6 of Table IV. The corresponding diagonalized eigenvalues and intensities appear in columns 7 and 8. After refinement to force a fit to the observed spectrum the zero order energies and interactions change to the values listed in columns 9 and 10. These yield the calculated spectrum of columns 11 and 12. They are to be compared with the observed spectrum tabulated in columns 1 and 2. These three stages are also shown in Figure 18.

The fit to the observed spectrum is so satisfactory that only slight interpretation is required. The general intensity distribution pattern can be explained on the basis of the $^1B_{2u}$ origin interacting primarily with the one strong vibronic level at 2400 cm^{-1}, ascribed to $b_{1g}(8) + 2 \times a_g(7)$. The 2320 cm^{-1} line appears, but with far less than the required 0.02 to 0.03 fractional intensity. It is a victim of out-of-phase intensity transfer, with 2293 and 2262 receiving the benefit of increased $H(1,2320)$ and $H(1,2322)$ (where the component state is referenced by its diagonal matrix element energy). These diagonalization phasing problems seem to be somewhat resistant to treatment by Jacobian techniques, requiring intuitive or trial and error adjustment. In this particular case, 2322 involves $a_g(4)$ excitation so that $^1B_{2u} + a_g(4)$ moment interference is expected although it is neglected in the calculation. Eigenvectors reflect the complex coupling in this region. Considerable patience and corresponding quantities of computer time are required to test enough coupling adjustments to balance intensities and energies properly. Even slight adjustments of single terms can cause drastic shifts in overall band patterns in the region 2266 to 2360 cm^{-1}. The intense bands at 2267 and 2294 are mixtures of several zero order levels, namely the $^1B_{2u}$

TABLE IV

Diagonalization of the vibronic Hamiltonian[a] for naphthalene in *p*-xylene

Observed[a] Spectrum in -Xylene $\Delta\bar{\lambda}$	Intensity[b]	Estimates to the unperturbed Spectrum and the Vibronic Coupling from First Order Perturbation Theory with one $^1B_{2u}$ Level			
		from *p*-xylene		from Durene	
		$H(n, n)$	$H(1, n)$[c]	$H(n, n)$	$H(1, n)$[d]
①	②	③	④	⑤	⑥
424 cm^{-1}	0.039	491 cm^{-1}	350 cm^{-1}	532 cm^{-1}	480 cm^{-1}[e]
903	0.028	939	220	933	230
1130	0.022	1153	160	1156	200
1419	0.020	1434	110	1437	160
1613	0.020	1625	82	1621	110
1842	0.012	1846	39	1851	91
1897	0.023	1904	44	1895	54
1917	0.057	Complete Mixing		1943	73
2125	0.017			2123	48
2260[f]	0.13			2274	22
2290[g]	0.11				
2319	0.03			2320	32
2343	0.066			2342	9
2359	0.12			2363	10
				2406	22
				2416	21
				2442	8
2441	0.014				
2462	0.028			2473	7
2482	0.20				
2498	0.015				
2515	0.005			2513	8
2533	0.011			2519	6
				2547	9
2558	0.028			2560	11
2603	0.007			2595	15
2644	0.046			2611	6
$^1B_{2u}$ 0, 0		2220		2740	

[a] Energies for lines above 2200 cm^{-1} are estimated from the intensity center of strong line groupings. Thus, 2260 refers to the group of three components near 2260 (refer to Figure 5) which has an intensity centroid at 2260 ± 3 cm^{-1}. The arguments used to justify grouping into a few strong component groups are given in the text. Only the strongest of the lines below 2200 cm^{-1} are given.

[b] Intensities are for the phononless lines. They have been normalized so that the integrated $^1B_{2u}$ 0,0 intensity is 1.0. The line intensities relative to neighboring lines should be accurate to 10% but the fractional intensity is very dependent on separation of phononless intensity from lattice intensity. Therefore, these values could be in error by 30%.

[c] The perturbation matrix elements $H(1, n)$ have been obtained from the intensity normalized to 1.0 for the $^1B_{2u}$ origin system by use of equation (3). The diagonal elements $H(1, 1)$ are the observed line positions corrected for the first order vibronic energy perturbation (Eq. 4) $\delta E = H(1, n)^2/\Delta E$, where ΔE is the separation between the line and the $^1B_{2u}$ band center. These estimates are restricted to the region where vibronic mixing of the zero-order Born–Oppenheimer components is small.

[d] Matrix elements are taken from durene because first order estimates of $H(n, n)$ and $H(1, n)$ extend into the resonance region of the *p*-xylene host. The $^1B_{2u}$ origin in durene is taken as 2750

TABLE IV—*Continued*

Using the Matrix Elements from Durene Listed in Columns 5 & 6			Using the Best Matrix Elements Obtained by Changing from the Values of Columns 5 & 6 Until the Observed Spectrum is Matched		Calculated[b]	
$\Delta\tilde{\lambda}$	Intensity	Assign.	$H(n, n)$	$H(1, n)$	$\Delta\tilde{\lambda}$	Intensity
(7)	(8)		(9)	(10)	(11)	(12)
414 cm^{-1}	0.045	8 0	489	318 cm^{-1}	424 cm^{-1}	0.039
895	0.026	7 0	944	230	903	0.029
1128	0.019	8 8	1156	190	1130	0.018
1414	0.020	8 7	1441	150	1419	0.020
1609	0.013	7 8	1623	90	1613	0.011
1837	0.022	8 8 + 8	1850	50	1843	0.017
1891	0.005	7 7	1900	20	1898	0.011
1936	0.010	8 3	1959	150	1917	0.062
2117	0.015	8 8 + 7	2134	55	2122	0.020
2271	0.016	8 8 + 6	2278	17	2262	0.16
		7 8 + 8	2281	27	2293	0.071
2313	0.047	8 9 + 5	2320	40	2321	0.000
2341	0.004	7 4	2322	50	2345	0.028
2362	0.011	8 9 + 4	2350	25	2364	0.083
2394	0.17	8 7 + 7	2400	80		
2412	0.023					
2440	0.069	7 3	2441	20	2438	0.020
2454	0.416					
2474	0.039		2465	15	2461	0.055
			2487	6	2479	0.20
		8 8 + 5	2504	9	2488	0.030
2514	0.007		2515	13	2505	0.010
2519	0.005					
2548	0.004	7 9 + 6	2546	20	2548	0.007
2561	0.006	8 8 + 4	2555	25	2560	0.030
2596	0.007	7 8 + 7	2608	30	2611	0.011
2611	0.001	8 8 + 3	2630	40	2638	0.036
			2879	50		
			3000	50		
		$^1B_{2u}$ 0, 0	2190			

cm^{-1}. Since the durene estimate for $b_{1g}(8)$ (532) appears unreliable, the *p*-xylene estimate has been used instead.

[e] This estimate seems unrealistically large. It causes the zero order $b_{1g}(8)$ frequency to exceed the ground state value of about 516 cm^{-1}. Overestimation of fractional intensity in the durene spectrum is the presumed cause. The *p*-xylene first order estimates seem more acceptable. Were the durene $b_{1g}(8)$ intensity 0.023, it would be consistent with the *p*-xylene result. An intensity 0.036 would be consistent with reduction of a zero order unperturbed $b_{1g}(8)$ energy 516 cm^{-1} to the observed 432.

[f] The component group whose most intense component is 2267 (Figure 5) has intensity centroid at 2260.

[g] The component group whose most intense component is 2294 has intensity centroid 2290.

[h] Interaction is limited to the $^1B_{2u}$ zero point level. No provision has been made for interference from the transition moment of a_g additions to the $^1B_{2u}$.

[i] Eigenvectors appear in Table V.

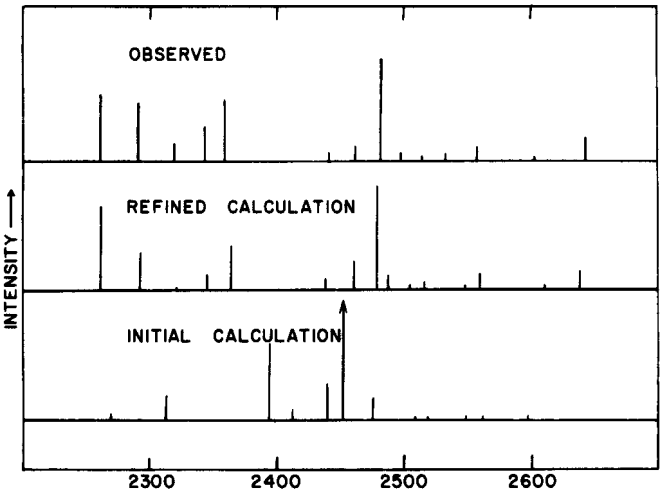

FIGURE 18 $^1B_{2u}$ origin system calculated for naphthalene-h_8. Intensities of the $^1B_{2u}$ origin system of naphthalene-h_8 in *p*-xylene predicted by the refined diagonalization are compared with the "observed" spectrum. The observed line intensities were obtained from the integrated areas of line groupings attributed to strong coupling combinations. The baseline is defined by the dashed line of Figure 5. Energies are relative to the $^1B_{3u}$ origin. The multiple components near 2267, 2294, and 2644 must be due to weak coupling components that are of interest in the calculation. Therefore, intensity is summed for each of these line systems. The initial calculation which appears at the bottom of the figure was made directly from the first order estimates to interaction parameters. The zero order parameters and final eigenfunctions are listed in Table IV columns 9 and 10, and Table V.

origin, 2278, 2281, 2322, 2350 and 2400. The combinations involved are: $b_{1g}(8) + a_g(8) + a_g(6)$; $b_{1g}(7) + a_g(5)$; $b_{1g}(7) + a_g(4)$; and $b_{1g}(8) + a_g(9) + a_g(5)$. Table V shows the first states in terms of the zero order basis states.

The 2320 to 2370 cm^{-1} region is attributed to $b_{1g}(7) + a_g(4)$ with very strong interaction, to $b_{1g}(8) + a_g(9) + a_g(5)$, and to $b_{1g}(8) + a_g(9) + a_g(4)$ with weaker interaction. The intensity at 2360 could belong primarily to the line at 2343 if the lattice baseline has been underestimated between 2350 and 2370 cm^{-1} and overestimated below 2350. If so, the coupling strength of the $b_{1g}(7) + a_g(4)$ combination must be stronger than assumed. The possibility of antiresonance structure in this region might cause 10 cm^{-1} errors in estimation of zero order line positions. Line positions and intensities near the intense $^1B_{2u}$ 0, 0 component at 2482 are sensitive to zero order $^1B_{2u}$ position and to all vibronic coupling strengths. They seem to be predicted accurately, although no lines are predicted at 2502 and 2530. Those to the high energy of the 2482 system have little mixing, therefore simple assignments. All major lines are generated with reasonable intensities by this iterative diagonalization procedure.

TABLE V

Vibronic eigenvectors naphthalene-h_8 in p-xylene

State Calc. (Obs.)	Zero Order B. O. Basis Components[a]
2262(7)	$0.40\|^1B_{2u}\rangle - 0.42\|2278\rangle - 0.56\|2281\rangle - 0.33\|2322\rangle$ (8, 8 + 6) (7, 8 + 8) (7, 4)
2278(9)	$0.85\|2278\rangle - 0.52\|2281\rangle$
2293(4)	$0.31\|2278\rangle + 0.62\|2281\rangle - 0.38\|2320\rangle - 0.45\|2322\rangle$ (8, 9 + 5)
2320(19)	$-0.78\|2320\rangle + 0.62\|2322\rangle$ (8, 9 + 5)
2345(5)	$-0.36\|2322\rangle + 0.83\|2350\rangle$ (7, 4) (8, 9 + 4)
2364(59)	$0.29\|^1B_{2u}\rangle + 0.34\|2322\rangle + 0.52\|2350\rangle - 0.64\|2400\rangle$ (8, 7 + 7)
2438(40)	$0.29\|2400\rangle - 0.93\|2441\rangle$ (8, 9 + 3)
2461(2)	$0.31\|2400\rangle - 0.86\|2465\rangle$
2479(82)	$-0.44\|^1B_{2u}\rangle - 0.45\|2400\rangle - 0.47\|2465\rangle + 0.33\|2487\rangle$
2488(90)	$-0.94\|2487\rangle$
2505(98)	$0.97\|2504\rangle$
2516(5)	$-0.97\|2514\rangle$ (8, 8 + 5)
2548(8)	$0.95\|2546\rangle$ (7, 9 + 6)
2560(58)	$0.93\|2555\rangle$ (8, 8 + 4)
2611(03)	$0.96\|2608\rangle$ (8, 9 + 8 + 7)
2638(44)	$-0.95\|2630\rangle$ (8, 8 + 3)

[a] The eigenvectors are denoted by the frequency of the zero order energies of column 9, Table IV.

f. Comparison of the observed low energy spectrum in durene with the zero order refined matrix elements

The zero order line energies, following refinement, seem to be related to their durene counterparts reasonably. These are in column 9 of Table IV. The $b_{1g}(8)$ false origin at 432 derives from a zero order vibration with energy 489 cm^{-1}, only 20 cm^{-1} below the ground state b_{1g} frequency. The small change between ground and excited zero order frequencies indicates that the $^1B_{3u}$ force field is remarkably similar to that of the ground state when vibronic interaction is absent. The same applies to the $b_{1a}(7)$ mode, which has an esti-

(column 10). Values of the electronic part of the coupling constant can be derived from these. The results in columns 9 and 10 give a detailed analysis of the vibronic coupling involving the $^1B_{3a}$ and $^1B_{2a}$ states. The coupling matrix elements could be further analyzed by partitioning them into the a_g overlap factor, the b_{1g} displacement factor and the electronic factor.

g. Results for naphthalene *d*-8

The same diagonalization applied to naphthalene *d*-8 in *p*-xylene gives results as satisfactory as for *h*-8, and with comparable energy shifts and interaction matrix elements for corresponding vibrational modes.

The matrix element $H(1, b_{1g}(8)) = 355$ cm^{-1}, somewhat larger than the value 318 cm^{-1} shown for *h*-8 in column 10 of Table IV. The larger value in *d*-8 may be caused by the mode changes expected on isotope substitution. These changes may also account for the appearance of $b_{1g}(1)$ and $b_{1g}(2)$ in *d*-8, whereas, they do not appear in *h*-8. The larger components of carbon motion in the *d*-8 modes would be the basic reason for these differences. The diagonalization also shows why $b_{1g}(6)$ is more intense than $b_{1g}(7)$ in *d*-8.

The consistency of these results with those for the *h*-8 molecule lends strong support to the validity of the entire analysis.

h. The a_g additions to $^1B_{2u}$

The complex line structure around the origin of the $^1B_{2u}$ spectrum is repeated at intervals corresponding to the a_g mode frequencies, as shown in Figures 10 and 11. The second group in durene repeats almost every feature of the first at 499.6 ± 1.7 cm^{-1} to higher energy. In *p*-xylene, repetitions are observed at 502 ± 5, 993 ± 6 and 1420 ± 11. For *d*-8 in *p*-xylene we find 481 ± 3, 830 ± 5 and 1396 ± 2. The three intervals are probably $a_g(9)$, $a_g(7)$ and $a_g(4)$ respectively.

The repetition of the patterns of the O, O region shows that for every a_g addition in $^1B_{2u}$ there is a similar set of secondary modes of $^1B_{3u}$ able to interact with it. The intensities of the O, O group, however, are not exactly reproduced in each higher group, as can be seen from the figures. These intensity variations can be reasonably explained in terms of the phase relations within the eigenvectors of the solutions of Eq. 2, and the relative phases of the moment sources, $^1B_{2u}$ 0, 0 and the $^1B_{2u} + a_g(n)$ additions.[1]

CONCLUSIONS

Our treatment of the naphthalene spectrum has encompassed both the

from the strict single component Born–Oppenheimer wavefunctions. Because of the semi-empirical adjustments made in the solution of Eq. 2, the final wavefunctions obtained are in a mixed basis in which the $^1B_{3u}$ and $^1B_{2u}$ components refer to their separate equilibrium nuclear configurations. These two states have very similar configurations, however. The calculations could be further refined if this were necessary for any future work where exact eigenfunctions were needed. The calculations presented here, and in more detail in Ref. 1 are enough to show that the entire problem of the interaction of the two states is tractable and in their present form they lead to the main results of physical interest.

References

1. John Wessel, Degenerate Vibronic Interference in Naphthalene, Doctoral Thesis, University of Chicago, Chicago, Illinois 60637, December 1970.
2. C. A. Langhoff and G. W. Robinson, *Chem. Phys.*, **6**, 34 (1974). G. W. Robinson and C. A. Langhoff, *Chem. Phys.*, **5**, 1 (1974).
3. H.-K. Hong, *Chem. Phys.*, **9**, 1 (1975).
4. D. S. McClure, *J. Chem. Phys.*, **22**, 1668 (1954), **24**, 1 (1956).
5. M. Kasha, *Disc. Faraday Soc.*, **9**, 14 (1950).
6. E. H. Gilmore, G. E. Gibson, and D. S. McClure, *J. Chem. Phys.*, **20**, 829 (1952).
7. R. Williams, *J. Chem. Phys.*, **28**, 577 (1958). R. Williams and G. J. Goldsmith, *J. Chem. Phys.*, **39** 2008 (1963).
8. S. G. Biswas, *Ind. J. Phys.*, **34**, 263 (1960).
9. D. E. Freeman and I. G. Ross, *Spectro Chim. Acta.*, **16**, 1393 (1960). Also see S. C. Scully and D. H. Whiffen, *ibid.* **16**, 1409 (1960).
10. D. P. Craig and G. J. Small, *J. Chem. Phys.*, **50**, 3827 (1969).
11. U. Fano, *Phys. Rev.*, **124**, 1866 (1961).